

Ultracold plasma expansion in quadrupole magnetic fieldS. Ya. Bronin, E. V. Vikhrov , B. B. Zelener , and B. V. Zelener**Joint Institute for High Temperatures of the Russian Academy of Sciences,
Izhorskaya Street 13, Building 2, Moscow 125412, Russia*

(Received 15 August 2023; accepted 4 October 2023; published 23 October 2023)

We present simulation results of ultracold Sr plasma expansion in a quadrupole magnetic field by means of molecular dynamics. An analysis of plasma evolution influenced by a magnetic field is given. Plasma confinement time behavior under variation of magnetic field strength is estimated. Similarity of the time dependence of the concentration and distribution of ion velocities against the parameters of the plasma and magnetic field is established. Simulation results are in agreement with the experimental ones.

DOI: [10.1103/PhysRevE.108.045209](https://doi.org/10.1103/PhysRevE.108.045209)**I. INTRODUCTION**

Studies of plasma confinement by means of magnetic fields were originally associated with the fusion energy program. Recently, new problems have arisen for which this problem is important, in particular, problems in astrophysics [1]. The quadrupole configuration of the magnetic field formed by coils with oppositely directed electric currents [2,3] can keep neutral plasma near the central region of the zero field due to the magnetic mirror effect [4]. This confinement scheme was initially of interest for magnetic confinement fusion [2,3,5–7] and, more recently, for ion sources, material processing, and ion propulsion systems [8–11].

New opportunities for studying magnetized and magnetically confined plasma particles are associated with ultracold plasma (UCP). UCP is obtained by means of photoionization of laser-cooled atoms (usually of an alkali or alkaline-earth metal) near the ionization threshold, in a magneto-optical trap in high vacuum, using a pulsed laser. In this case, the UCP [12,13] is short lived with a maximum density of 10^{10} cm^{-3} and its lifetime is approximately 100 μs . This plasma has ion temperatures $T_i \sim 1 \text{ K}$ and tunable electron temperatures $T_e = 1\text{--}1000 \text{ K}$. In this connection, the UCP makes it possible to study the combined effect of magnetization and strong coupling on collision processes and transport processes. The ratio of the Coulomb energy to the kinetic energy, known as the Coulomb coupling parameter [14], can reach unity for electrons and 10 for ions [15–17]. In addition, the UCP is not a neutral plasma due to the evaporation of some of the electrons at the initial moment of its formation. As a result, a radial electric field arises in it, which, together with the magnetic field, is a trap for the remaining electrons.

The UCP in a magnetic field was experimentally studied in [18–24]. Similar methods were also used in order to confine partially overlapping clouds of positive and negative charges at ultralow temperatures in nested traps, for example, for antihydrogen production [21,22].

In [23], the expansion of the UCP cloud of Ca atoms in a uniform magnetic field was experimentally studied at various magnetic induction values from 0 to 0.123 T. Experimental

time dependencies of the plasma dimensions were obtained for various values of the magnetic field induction. The dependencies of the plasma expansion rate on the value of magnetic induction were also determined and empirical expressions were proposed. In [24], the expansion of the UCP cloud of Sr atoms in a quadrupole magnetic field with a magnetic induction gradient $B = 150 \text{ G/cm}$ was experimentally studied. The initial electron temperature $T_e = 20, 40, 160 \text{ K}$, and the initial density $n_0 = (1.5\text{--}3.9) \times 10^9 \text{ cm}^{-3}$. The number of ions in the plasma was approximately 10^8 . The initial configuration of the plasma cloud was determined by the cylindrical shape of the cloud of atoms in a quadrupole magnetic field. By means of processing the fluorescence spectra of ions, the distributions of the concentration and velocities of ions along the symmetry axes in the projection onto the plane were obtained at various times. Average ion concentrations at various times were determined as well. It turned out that the quadrupole magnetic field contributes to slowing down the ion expansion velocity during the observation time, compared to expansion without a field. This leads to an increase in the concentration of ions at the corresponding time points. Furthermore, the confinement time of the UCP for the above-said parameters approaches 0.5 ms, while unmagnetized plasmas dissipate on a timescale of several dozens of microseconds.

In this paper, we simulate the expansion of two-component ultracold Sr plasma with initial cylindrical density distribution in a quadrupole magnetic field by means of molecular dynamics. The selected simulation parameters are close to those of experiments [24]. Similarity of the time dependence of the plasma concentration on the parameters of the plasma and the magnetic field is established. An analysis of plasma evolution influenced by a magnetic field is carried out. The dynamics of both charge types is studied. An estimate of plasma confinement time and plasma density under various magnetic field strength is given. Satisfactory agreement with experiment is obtained.

II. SIMULATION DETAILS

In this paper, the UCP expansion in a quadrupole magnetic field is simulated by means of the molecular dynamics for the number of particles much less than that in the experiment. The simulation parameters are chosen such that the obtained

*bzelener@mail.ru

characteristics are similar to the experimental characteristics. In previous papers [25,26], the same problem was solved in the absence of a magnetic field. The initial kinetic energy of electrons is determined by means of the excess of the ionizing radiation energy over the ionization energy. Real particle masses are used. A configuration with cylindrical symmetry is chosen as the initial shape of the plasma cloud, similarly to the experimental configuration [24]. The simulations were performed for initial temperatures of electrons of $T_{e0} = 20$ and 200 K and initial temperature of Sr ions of $T_{i0} = 10^{-3}$ K. Charge number density n varies from 1×10^9 to 3×10^9 cm $^{-3}$. The number of ions and electrons is $N_i = N_e = 10^4$, which is three to four orders of magnitude less than the experimental value. The magnetic field gradient B' varies from 1.5×10^3 to 3×10^4 G/cm, which differs from experimental values. We give an explanation of it in Sec. III. Some simulations were performed without a magnetic field.

The free expansion of plasma in the magnetic field of two oppositely directed ring currents is considered. When the distance to the center is less than the distance between the circular currents, the magnetic field depends linearly on the coordinates,

$$B_x \approx B'x, \quad B_y \approx -\frac{1}{2}B'y, \quad B_z \approx -\frac{1}{2}B'z. \quad (1)$$

A modification of the leapfrog integration method is used. This scheme accounts for the magnetic field properly,

$$\begin{aligned} \mathbf{r}_{i+1}^\alpha &= \mathbf{r}_i^\alpha + \mathbf{v}_i^\alpha \Delta t + \frac{(\Delta t)^2 q^\alpha}{2m^\alpha} \left(\mathbf{E}_i^\alpha + \frac{1}{c} [\mathbf{v}_i^\alpha, \mathbf{B}_i^\alpha] \right), \\ \mathbf{v}_{i+1}^\alpha &= \frac{\mathbf{u}_i^\alpha + \Delta t [\mathbf{u}_i^\alpha, \mathbf{w}_i^\alpha] + (\Delta t)^2 \mathbf{w}_i^\alpha (\mathbf{u}_i^\alpha, \mathbf{w}_i^\alpha)}{1 + (\Delta t w_i^\alpha)^2}, \end{aligned} \quad (2)$$

where \mathbf{w} is

$$\mathbf{w}_i^\alpha = \frac{q}{2m^\alpha c} \mathbf{B}_{i+1}^\alpha, \quad (3)$$

and \mathbf{u} is

$$\mathbf{u}_i^\alpha = \mathbf{v}_i^\alpha + \frac{\Delta t q^\alpha}{2m^\alpha} \left(\mathbf{E}_i^\alpha + \mathbf{E}_{i+1}^\alpha + \frac{1}{c} [\mathbf{v}_i^\alpha, \mathbf{B}_{i+1}^\alpha] \right). \quad (4)$$

Here, i is the number of step, Δt is the size of each time step, c is the speed of light, α is type of a particle, $q^\alpha = \pm e$ is its charge, and m^α is its mass. The electric field strength is $\mathbf{E}_i^\alpha = \mathbf{E}(\mathbf{r}_i^\alpha)$ and the magnetic field induction is $\mathbf{B}_i^\alpha = \mathbf{B}(\mathbf{r}_i^\alpha)$.

Since calculation of particle-particle interactions accounts for all of them, the computational complexity is $O(N^2)$. To perform simulation, a parallel algorithm was developed.

III. SIMILARITY PARAMETERS

Parameters of the present simulation differ from the parameters of the experiment [24] in the number of particles and, accordingly, in the initial plasma size σ_0 , which in our simulation ($\sigma_0 = 0.015$ cm) is only one-tenth of the experimental size. Comparison of the simulation results with experimental results is possible due to the self-similar nature of the time dependence of the expanding plasma parameters, established in [24]. Such quantities as plasma size $\sigma(t)$ and concentration $n_i(t)$, made dimensionless against their initial values σ_0 and n_{i0} , are standard functions of dimensionless time, whose characteristic scale is the ratio of the initial plasma size σ_0 to

the characteristic expansion velocity $V_T = \sqrt{kT_{e0}/m_i}$: $\tau_{\text{exp}} = \sigma_0/V_T$. For adequate simulation of plasma expansion in the presence of a magnetic field, it is necessary to determine the ratio of the calculated and experimental values of B' , which would make it possible to compare the results of simulation with experiment. During the initial stage of plasma evolution, the magnetic field does not significantly affect the process of expansion due to the small size of the plasma cloud. The expansion is mainly influenced by the electric field formed by charge imbalance which arises as a result of evaporation of a fraction of the electrons. The later stages of plasma evolution are characterized by a predominant influence of magnetic field. The depth of the potential well decreases with time in inverse proportion to the plasma size. The magnetic field induction increases in direct proportion to this size. At later times the electrical interaction can be neglected. By choosing σ_0 , V_T , and τ_{exp} as units of length, velocity, and time, respectively, we obtain dimensionless units $\boldsymbol{\xi} = \mathbf{r}/\sigma_0$, $\mathbf{u} = \mathbf{v}/V_T$, and $\tau = t/\tau_{\text{exp}}$. For the ionic distribution function, one can write

$$\frac{\partial f_i}{\partial \tau} + \mathbf{u} \frac{\partial f_i}{\partial \boldsymbol{\xi}} + \beta [\mathbf{u}\mathbf{b}] \frac{\partial f_i}{\partial \mathbf{u}} = 0, \quad (5)$$

where $\mathbf{b} = \mathbf{B}/B'\sigma_0$ and $\beta = eB'\sigma_0^2 \sqrt{m_i k T_{e0}}/c$.

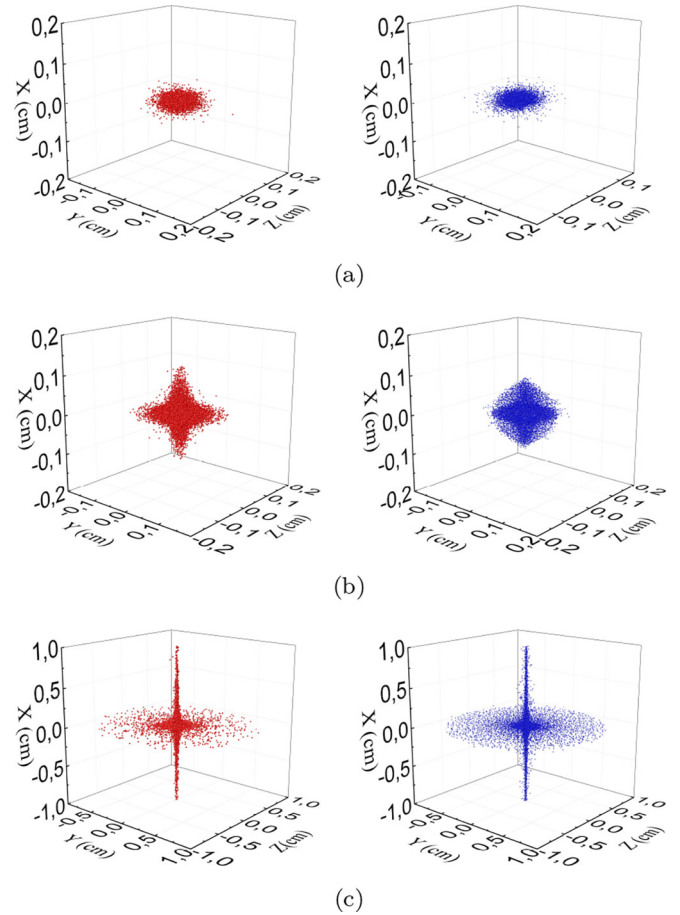


FIG. 1. Snapshots of electrons (left) and ions (right) for $T_{e0} = 20$ K, $N_e = N_i = 10^4$, $n = 10^9$ cm $^{-3}$, $B' = 3 \times 10^3$ G/cm at different times: (a) $t/\tau_{\text{exp}} = 0$, (b) $t/\tau_{\text{exp}} = 3$, (c) $t/\tau_{\text{exp}} = 63$.

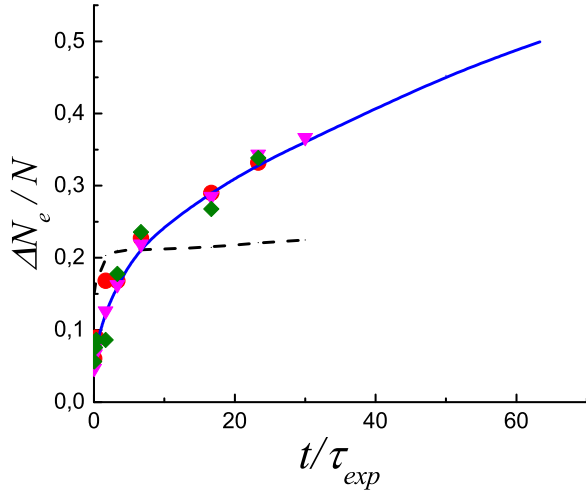


FIG. 2. Time dependence of charge imbalance. $T_{e0} = 20$ K, $N_e = N_i = 10^4$, $n = 10^9$ cm $^{-3}$, and various magnetic field strength values $B' = 0$ G/cm (dashed line), $B' = 1 \times 10^3$ G/cm (circle), $B' = 3 \times 10^3$ G/cm (solid line), $B' = 6 \times 10^3$ G/cm (triangle), $B' = 1.5 \times 10^4$ G/cm (rhombus).

The value of B' during the simulation should be chosen such that the dimensionless parameter β would coincide with the experimental value. Note that the ratio of the Larmor radius of the electron in the field $B \sim B'\sigma_0$ to the characteristic plasma size σ_0 is determined by the same parameter and is equal to $\sqrt{m_e/m_i}/\beta$.

In the experiment, T_e varies from 40 to 160 K. We choose $T_e = 20$ K for the simulation. For the chosen temperature and the ratio of simulated to experimental plasma sizes mentioned earlier, the values of the similarity parameter β was changed in the interval $0.1\beta_{\text{exp}} < \beta < 2\beta_{\text{exp}}$. Here, β_{exp} is the value of this parameter corresponding to the experimental conditions. Thus the simulations were performed with the magnetic field gradient values in the range $B' = 1.5 \times 10^3$ to 3×10^4 G/cm. Such interval of B' corresponds to the magnetic field strength gradient $B = 150$ G/cm in the experiment.

IV. PLASMA EVOLUTION

The data obtained as a result of simulation make it possible to present the physical picture of the expansion both for electrons and for ions. Figure 1 show particle snapshots for three time points at $T_{e0} = 20$ K, $N_e = N_i = 10^4$, $n = 10^9$ cm $^{-3}$, $B' = 3 \times 10^3$ G/cm. Figure 1(a) shows the initial configuration of the system. As mentioned above, it has cylindrical symmetry as well as the experimental configuration [24]. Figure 1(b) shows the configuration of electrons and ions at the time when the influence of the magnetic field on the ions begins to dominate over the effect of the electric trap. Thus the magnetic field affects the shape of the system. Due to the large difference in masses, this effect in the case of ions is considerably less pronounced compared with that for the electrons at the same time point. As we have previously shown [25,26], when the plasma cloud expands in the absence of a magnetic field, an ion wave arises due to the charge imbalance, which drags the plasma along and contributes to its expansion. However, with an increase in the size of the

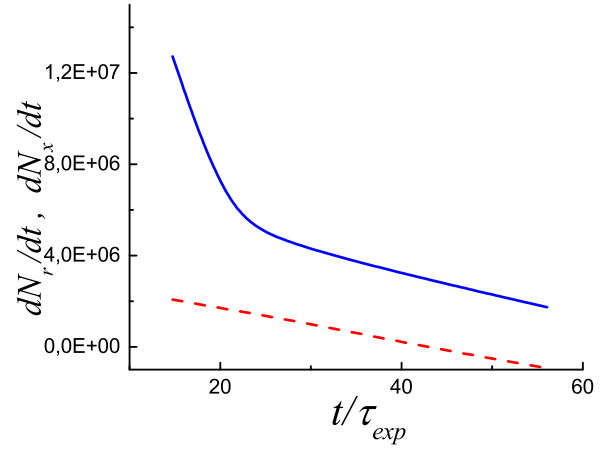


FIG. 3. Time dependence of the ion flux through the cylinder $r < 5\sigma_0$, $|x| = 2.5\sigma_0$ at $B' = 10^4$ G/cm: the ion flux dN_x/dt through the bases (dashed line) and the ion flux dN_r/dt through the lateral surface (solid line).

plasma, the quadrupole magnetic field at some time begins to slow down the electrons, and the electrons begin, in their turn and with some delay, to slow down the ions. This results in a change in the nature of the expansion compared to the expansion without a magnetic field.

Figure 1(c) shows the particles at later times when the depth of the potential well decreases due to plasma expansion. Since electrical interactions are no longer significant, some of the fastest electrons and ions leave the plasma region along the magnetic field lines. The remaining part of the plasma is located in the central region and expands much more slowly compared to the case of the absence of the magnetic field.

Charge imbalance in the plasma changes with time. Here, the plasma is understood as a region where all $N_i = 10^4$ ions and $N_e < 10^4$ remaining electrons are present. Other ΔN_e

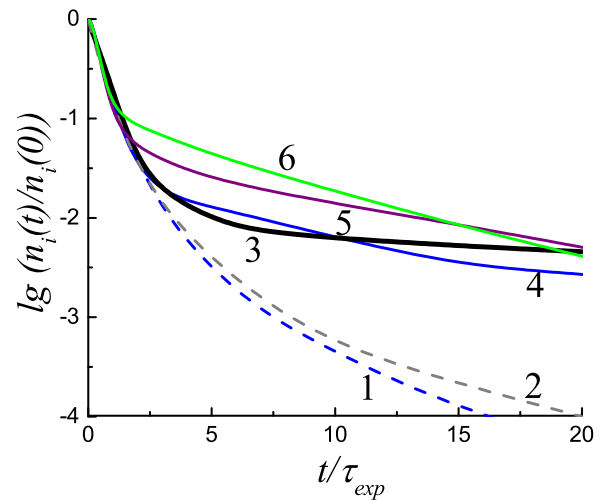


FIG. 4. Time dependence of $\lg[n_i(t)/n_i(0)]$ at different magnetic field gradients and $T_e = 20$ K for the experimental (2, 3) and simulations (1, 4, 5, 6) data. 1: $B' = 0$; 2: $B = 0$ [24]; 3: $B = 150$ G/cm [24]; 4: $B' = 3 \times 10^3$ G/cm; 5: $B' = 10^4$ G/cm; 6: $B' = 3 \times 10^4$ G/cm.

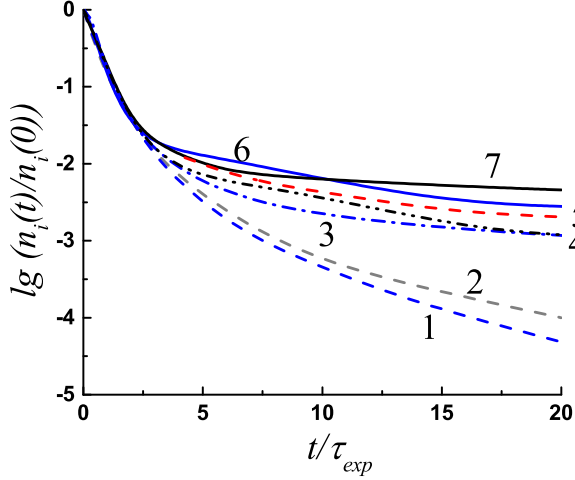


FIG. 5. Time dependence of $\lg[n_i(t)/n_i(0)]$ for the experimental (2, 5, 7) and simulations (1, 3, 4, 6) data. 1: $B' = 0$ G/cm; 2: $B = 0$ G/cm [24]; 3: $B' = 3 \times 10^3$ G/cm, $T_{e0} = 200$ K, $n_i(0) = 10^9$ cm $^{-3}$, $\tau_{\text{exp}} = 1.1$ μ s; 4: $B' = 3 \times 10^3$ G/cm, $T_{e0} = 20$ K, $n_i(0) = 3 \times 10^9$ cm $^{-3}$, $\tau_{\text{exp}} = 2.4$ μ s; 5: $B = 150$ G/cm [24], $T_{e0} = 160$ K, $n_i(0) = (1.5\text{--}3.7) \times 10^9$ cm $^{-3}$; 6: $B' = 3 \times 10^3$ G/cm, $T_{e0} = 20$ K, $n_i(0) = 10^9$ cm $^{-3}$, $\tau_{\text{exp}} = 3.4$ μ s; 7: $B' = 150$ G/cm [24], $T_{e0} = 40$ K, $n_i(0) = (1.5\text{--}3.9) \times 10^9$ cm $^{-3}$.

electrons are located at a distance much greater than the size of the plasma and do not affect its movement. Figure 2 shows the time dependence of the charge imbalance at $B = 0$ for different magnetic induction gradients in the case $T_{e0} = 20$ K, $N_e = N_i = 10^4$, and $n = 10^9$ cm $^{-3}$.

Distinct to expansion without a magnetic field, the charge imbalance in a magnetic field initially grows more slowly over time but then continues to grow, while without a magnetic field the charge imbalance reaches its limit. That is, plasma in a magnetic field becomes more charged over time. Moreover, this dependence on time is the same for different values of the magnetic field gradient within the considered range. To estimate the character of diffusion of charged particles in an inhomogeneous magnetic field, the particles' flux through the cylinder surface was calculated. The dimensions of the cylinder are fixed and amount to $r < 5\sigma_0$, $|x| = 2.5\sigma_0$. We choose a fixed area size because the area of measurements in the experiment is fixed as well. Figure 3 shows the time dependencies of the ion flux dN_x/dt through the bases of the cylinder along the symmetry axis and the ion flux dN_r/dt through its lateral surface. The negative value of dN_x/dt starting at $t/\tau_{\text{exp}} \approx 40$ means that the ions that escaped along the x axis begin to return and after that, the particles leave through the lateral surface only.

V. COMPARISON WITH EXPERIMENT

In [24], UCP expansion in a quadrupole magnetic field was studied experimentally. One of the main results is the influence of the magnetic field on the time dependence of the ion density. Contrary to the UCP expansion without a magnetic field, the decrease in the ion density sharply slows down over time and the plasma lifetime thereby increases.

While the experiment provides diagnostics of ions, simulation allows one to diagnose the electrons as well as the ions. This is very useful for a better understanding of the physics of the studied process.

In [25], the results of simulation of the UCP expansion without a magnetic field were presented. Figure 4 shows the calculated UCP density in relation to its initial value and the experimental results at $T_e = 20$ K.

Figure 4 also shows the experimental curve for $B = 150$ G/cm, which initially coincides with the curve for $B' = 0$, and then, at $t/\tau_{\text{exp}} \approx 3$, changes its character due to the increased influence of the magnetic field on the UCP expansion. The calculated curve for $B' = 3 \times 10^3$ G/cm shown in Fig. 4 corresponds to the average value in the above-said range of B' . Calculations for $B' = 3 \times 10^4$ G/cm [dashed curve (6)] show that the confinement time does not increase when B' grows threefold.

It was shown in [24] that there was a weak dependence of $n_i(t)/n_i(0)$ at a fixed B' on the initial values of density and temperature. Figure 5 shows the experimental data for $T_{e0} = 160$ and $T_{e0} = 40$ K (curves 5 and 7). Results of our

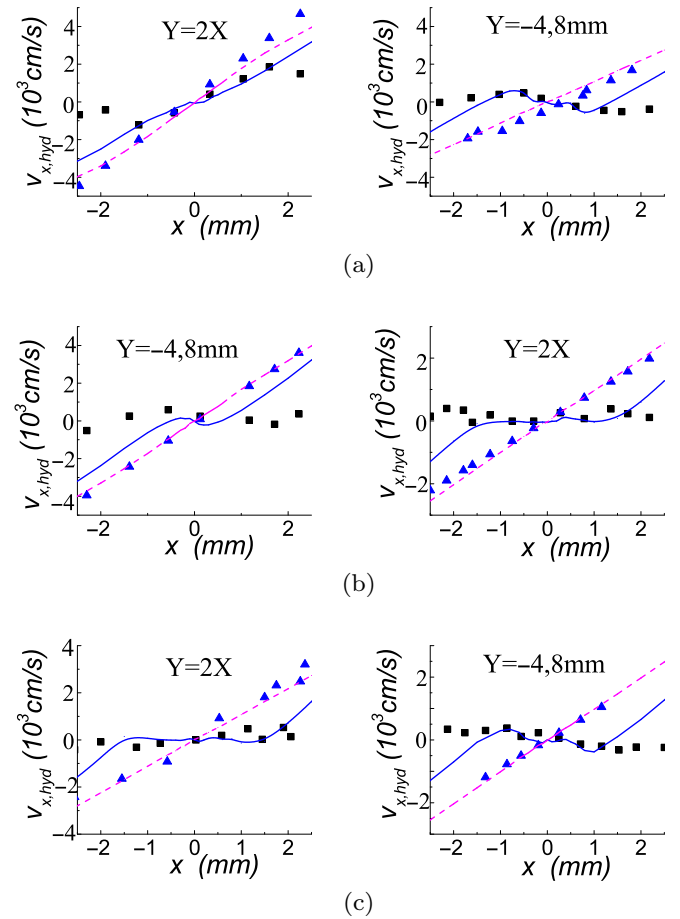


FIG. 6. Dependence of $v_{x,\text{hyd}}(x)$, averaged over the z coordinate at $y = 2x$ (left) and $y = -4.8$ mm (right). Here, $B = 150$ G/cm, data of [24] (squares); $B = 0$ G/cm, data of [24] (triangles); $B' = 3 \times 10^3$ G/cm, simulations data (solid line); $B' = 0$ G/cm, simulations data (dashed line) at different times: (a) $t/\tau_{\text{exp}} = 1.87$ ($t = 56$ μ s), (b) $t/\tau_{\text{exp}} = 2.83$ ($t = 85$ μ s), (c) $t/\tau_{\text{exp}} = 3.7$ ($t = 111$ μ s).

calculations within approximately the same range of changes for $n_i(0)$ and T_{e0} at $B' = 3 \times 10^3$ G/cm, shown in Fig. 5 (curves 3, 4, 6), confirm this.

Figure 6 shows a comparison with the experimental data [24] of the calculated values of $v_{x,\text{hyd}}$, averaged over z at fixed values of x and y at $y = 2x$ and $y = -4.8$ mm with a magnetic field $B' = 3 \times 10^3$ G/cm and without a magnetic field for three values of the expansion time.

A noticeable discrepancy between the simulations and experimental data for large absolute values of x in the presence of the magnetic field may be because the main contribution to the measured velocity values here comes from fast ions that have left the plasma. Since the number density of such ions is low, it should affect the accuracy of the measurements.

VI. CONCLUSION

In this paper, the dynamics of both plasma charges is studied. The results of simulation are in agreement with the experimental data [24]. The plasma confinement time increases the influence of the quadrupole magnetic field, which is in agreement with the experimental observations. However, this effect tends to saturate while B' increases. Thus,

confinement time does not significantly increase if the magnetic field strength increased.

It is shown that plasma is mostly located around the axis of symmetry and the horizontal plane of symmetry of a cylinder. The dynamics of expansion demonstrates that particles tend to expand along these two areas. Finally, the charge imbalance grows under the influence of a magnetic field compared to the free expansion of plasma.

Agreement between the provided results and the experimental data shows the similarity of plasma characteristics with the same values of t/τ_{exp} , which was established by the authors of [24].

ACKNOWLEDGMENTS

The theoretical investigations were supported by the Russian Science Foundation Grant No. 23-72-10031. The development of the computational code was supported by the Ministry of Science and Higher Education of the Russian Federation (State Assignment No. 075-01129-23-00). The calculations were performed on the hybrid supercomputer K60 installed in the Supercomputer Centre of Collective Usage of KIAM RAS.

-
- [1] A. H. Boozer, *Rev. Mod. Phys.* **76**, 1071 (2005).
 - [2] J. Berkowitz, K. Friedrichs, H. Goertzel, H. Grad, J. Killeen, and E. Rubin, *J. Nucl. Energy* **7**, 292 (1958).
 - [3] M. Sodha, S. Guha, A. Simon, and W. Thomas, *Physics of Colloidal Plasma, Advances in Plasma Physics Vol. 4* (Wiley, New York, 1971).
 - [4] R. Post, R. Ellis, F. Ford, and M. Rosenbluth, *Phys. Rev. Lett.* **4**, 166 (1960).
 - [5] M. Haines, *Nucl. Fusion* **17**, 811 (1977).
 - [6] A. Kitsunezaki, M. Tanimoto, and T. Sekiguchi, *Phys. Fluids* **17**, 1895 (1974).
 - [7] K. Leung, N. Hershkowitz, and K. MacKenzie, *Phys. Fluids* **19**, 1045 (1976).
 - [8] M. Carr, D. Gammersall, S. Cornish, and J. Khachan, *Phys. Plasmas* **18**, 112501 (2011).
 - [9] C. Cooper, D. Weisberg, I. Khalzov, J. Milhone, K. Flanagan, E. Peterson, C. Wahl, and C. Forest, *Phys. Plasmas* **23**, 102505 (2016).
 - [10] A. Hubble, E. Barnat, B. Weatherford, and J. Foster, *Plasma Sources Sci. Technol.* **23**, 022001 (2014).
 - [11] C. Russell, *IEEE Trans. Plasma Sci.* **28**, 1818 (2000).
 - [12] T. C. Killian, T. Pattard, T. Pohl, and J. Rost, *Phys. Rep.* **449**, 77 (2007).
 - [13] M. Lyon and S. Rolston, *Rep. Prog. Phys.* **80**, 017001 (2017).
 - [14] S. Ichimaru, *Rev. Mod. Phys.* **54**, 1017 (1982).
 - [15] C. E. Simien, Y. C. Chen, P. Gupta, S. Laha, Y. N. Martinez, P. G. Mickelson, S. B. Nagel, and T. C. Killian, *Phys. Rev. Lett.* **92**, 143001 (2004).
 - [16] M. Lyon, S. D. Bergeson, and M. S. Murillo, *Phys. Rev. E* **87**, 033101 (2013).
 - [17] T. K. Langin, G. M. Gorman, and T. C. Killian, *Science* **363**, 61 (2019).
 - [18] X. L. Zhang, R. S. Fletcher, S. L. Rolston, P. N. Guzdar, and M. Swisdak, *Phys. Rev. Lett.* **100**, 235002 (2008).
 - [19] X. L. Zhang, R. S. Fletcher, and S. L. Rolston, *Phys. Rev. Lett.* **101**, 195002 (2008).
 - [20] D. H. Dubin and T. O'neil, *Rev. Mod. Phys.* **71**, 87 (1999).
 - [21] G. Gabrielse, P. Laroche, D. Le Sage, B. Levitt, W. S. Kolthammer, R. McConnell, P. Richerme, J. Wrubel, A. Speck, M. C. George *et al.*, *Phys. Rev. Lett.* **100**, 113001 (2008).
 - [22] G. Gabrielse, N. S. Bowden, P. Oxley, A. Speck, C. H. Storry, J. N. Tan, M. Wessels, D. Grzonka, W. Oelert, G. Schepers *et al.*, *Phys. Rev. Lett.* **89**, 213401 (2002).
 - [23] R. T. Sprenkle, S. D. Bergeson, L. G. Silvestri, and M. S. Murillo, *Phys. Rev. E* **105**, 045201 (2022).
 - [24] G. M. Gorman, M. K. Warrens, S. J. Bradshaw, and T. C. Killian, *Phys. Rev. Lett.* **126**, 085002 (2021).
 - [25] E. Vikhrov, S. Y. Bronin, A. Klayrfeld, B. Zelener, and B. Zelener, *Phys. Plasmas* **27**, 120702 (2020).
 - [26] E. V. Vikhrov, S. Y. Bronin, B. B. Zelener, and B. V. Zelener, *Phys. Rev. E* **104**, 015212 (2021).